CENTRAL DIFFERENCE METHOD FOR REAL-TIME SUBSTRUCTURE TEST CONSIDERING SPECIMEN MASS

B. Wu[1], L.X. DENG[2] and X.D. Yang[3]

[1] *Professor, School of Civil Engineering, Harbin Institute of Technology, Harbin 150090, China*
[2] *Doctor Student, School of Civil Engineering, Harbin Institute of Technology, Harbin 150090, China*
[3] *Assistant Engineer, China Southwest Architectural Design and Research Institute, Chengdu 610081, China*
Email: bin.wu@hit.edu.cn, denglixia_my@163.com, yangxd_tom@163.com

ABSTRACT :

This paper studies the stability of the central difference method (CDM) for real-time substructure test considering specimen mass. To obtain correct reaction inertia force, an explicit acceleration formulation is assumed for the CDM. The analytical work shows that the stability of the algorithm decreases with increasing specimen mass if the experimental substructure is a pure mass. The algorithm becomes unstable whatever the time integration interval, i.e. unconditionally unstable, when the mass of specimen equal or greater than that of its numerical counterpart. For the case of dynamic specimen, the algorithm is unconditionally unstable when there is no damping in the whole test structure; a damping will make the algorithm stable conditionally. Part of the analytical results is validated by an actual test.

KEYWORDS: real-time substructure test, stability, inertia force, central difference method

1. INTRODUCTION

Real-time substructure testing (RSTing) is a hybrid approach to evaluate dynamic performance of structures. As a core element of the analytical part of RSTing, numerical integration plays a key role in a successful test. Most numerical integration algorithms in RSTing (Williams et al., 2001) are originated from the pseudo-dynamic testing (PDT). Many integration methods popular in PDT are explicit only for displacement. When an explicit velocity is required for damping specimen in RSTs, some extra formulation has to be assumed. This assumption very possibly does not conform to the original velocity formulation and this may change the numerical behavior of the integration algorithm. For the CDM in RSTing with damping specimen, Wu et al. (2005) showed that the stability decreases with increasing damping of the experimental substructure, contrasting constant stability limit of standard CDM. Similar problem may exist for implicit algorithm implemented in a RST. Wu et al. (2007) found that Newmark average acceleration method may lose the unconditional stability for damping specimen.

For a dynamic experimental substructure, the loading fashion should be explicitly and properly specified to obtain correct reaction of the substructures due to its inertia as well as stiffness and damping. This may change the numerical behavior of integration algorithms which normally do not include any explicit expressions for acceleration. Nguyen and Dorka (2006) showed that the Newmark average acceleration method became conditionally stable when the loading commands for the dynamic substructure were send off as a linear ramp function of time. Although there have been successful applications of explicit algorithms to inertia specimen and some discussions on stability related to time delay (Horiuchi and Konno, 2001) or coupling between numerical and experimental substructures (Bursi et al, 2007)), the impact of specimen mass on the stability of a specific integration method has not been explored. This paper will focus on the stability issue of the CDM arising in its implementation to RSTing with dynamic experimental substructure.

2. FORMULATION OF THE CDM FOR RST CONSIDERIING SPECIMEN MASS

In an RST, the acceleration-dependent force and velocity-dependent force exhibited by the specimen are introduced into the measured reaction force together with the static restoring force when the specimen is a dyn-

amic substructure. Therefore, the time-discretized equations of motion of the numerical substructure at the *i*th time step in an RST can be expressed in a more general and precise form as

$$\mathbf{M}_{\mathrm{N}}\mathbf{a}_{\mathrm{N},i}+\mathbf{C}_{\mathrm{N}}\mathbf{v}_{\mathrm{N},i}+\mathbf{K}_{\mathrm{N}}\mathbf{d}_{\mathrm{N},i}+\mathbf{R}_{\mathrm{E}}(\mathbf{a}_{\mathrm{C},i},\mathbf{v}_{\mathrm{C},i},\mathbf{d}_{\mathrm{C},i})=\mathbf{F}_i \tag{2.1}$$

and, when the CDM is employed, the velocity and acceleration are approximated by

$$\mathbf{v}_{\mathrm{N},i}=\frac{\mathbf{d}_{\mathrm{N},i+1}-\mathbf{d}_{\mathrm{N},i-1}}{2\Delta t} \tag{2.2}$$

$$\mathbf{a}_{\mathrm{N},i}=\frac{\mathbf{d}_{\mathrm{N},i+1}-2\mathbf{d}_{\mathrm{N},i}+\mathbf{d}_{\mathrm{N},i-1}}{\Delta t^2} \tag{2.3}$$

where **M**, **C** and **K** are the mass, damper and stiffness matrices of the numerical substructure respectively; **R** is the reaction force; **a**, **v** and **d** are acceleration, velocity and displacement vectors; **F** is external exciting on the numerical substructure; Δt is the integration time interval; subscripts N, E and C denote numerical substructure, experimental substructure and coupling degree-of-freedom of numerical and experimental substructures, respectively. Substituting Equations (2.2) and (2.3) into (2.1) gives

$$\mathbf{d}_{\mathrm{N},i+1}=\left(\frac{\mathbf{M}_{\mathrm{N}}}{\Delta t^2}+\frac{\mathbf{C}_{\mathrm{N}}}{2\Delta t}\right)^{-1}\left[\mathbf{F}_i-(\mathbf{K}_{\mathrm{N}}-\frac{2\mathbf{M}_{\mathrm{N}}}{\Delta t^2})\mathbf{d}_{\mathrm{N},i}-\left(\frac{\mathbf{M}_{\mathrm{N}}}{\Delta t^2}-\frac{\mathbf{C}_{\mathrm{N}}}{2\Delta t}\right)\mathbf{d}_{\mathrm{N},i-1}-\mathbf{R}_{\mathrm{E}}(\mathbf{a}_{\mathrm{C},i},\mathbf{v}_{\mathrm{C},i},\mathbf{d}_{\mathrm{C},i})\right] \tag{2.4}$$

To obtain accurate dynamic reaction force, the velocity and acceleration on the coupling degree-of-freedom at the (*i*+1)th step, which denoted by $\mathbf{v}_{\mathrm{c},i+1}$ and $\mathbf{a}_{\mathrm{c},i+1}$ respectively, have to be determined and imposed onto the specimen together with $\mathbf{d}_{\mathrm{c},i+1}$. This just can not be realized through Equations (2.2) and (2.3), as the displacement at the (*i*+2)th step is not yet available. For an actuator controlled in a traditional displacement mode, the achievement of the explicit velocity or acceleration target is dependent on how the displacement command is issued with respect with time. To this end, we assume a constant acceleration in the time interval from t_{i} to $t_{\mathrm{i+1}}$, resulted in by a displacement command profile as a quadratic function in time:

$$\mathbf{d}_{\mathrm{C},i+1}(t)=\mathbf{d}_{\mathrm{C},i}+\mathbf{v}_{\mathrm{C},i}\left(t-t_i\right)+\frac{1}{2}\tilde{\mathbf{a}}_{\mathrm{C},i+1}\left(t-t_i\right)^2 \tag{2.5}$$

in which the hat mark denotes target for loading. Note that, for seismic tests, the commands should include the ground motion to guarantee an absolute acceleration input to the dynamic specimen and hence obtain correctly reaction force due to inertia. Substituting Equation (2.2) into the above equation and letting $t=t_{i+1}$ entail

$$\tilde{\mathbf{a}}_{\mathrm{C},i+1}=\frac{\mathbf{d}_{\mathrm{C},i+1}-2\mathbf{d}_{\mathrm{C},i}+\mathbf{d}_{\mathrm{C},i-1}}{\Delta t^2} \tag{2.6}$$

By differentiating Equation (2.5) and utilizing Equations (2.2) and (2.6), we obtain

$$\tilde{\mathbf{v}}_{\mathrm{C},i+1}=\frac{3\mathbf{d}_{\mathrm{C},i+1}-4\mathbf{d}_{\mathrm{C},i}+\mathbf{d}_{\mathrm{C},i-1}}{2\Delta t} \tag{2.7}$$

Comparing Equations (2.7) and (2.6) with (2.2) and (2.3), we see that the velocity and acceleration at the coupling degree-of freedom of the experimental substructure is obviously no longer consistent to those of numerical substructure determined by the standard CDM. This raises the issue of possible change of numerical behavior, especially the stability, of the modified CDM over the standard one, which will be discussed next.

3. STABILITY ANALYSIS

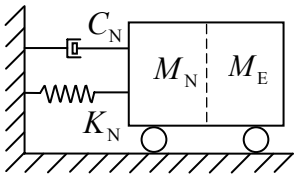

Figure 1 Computation schematic of structure in RST with pure inertia specimen

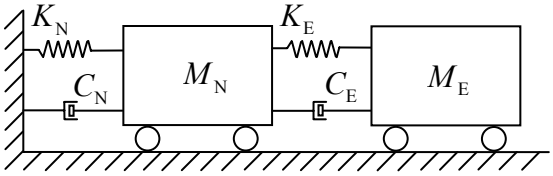

Figure 2 Computation schematic of structure in RST with dynamic specimen

We restrain our discussion within linear systems and the numerical substructure is of single-degree-of-freedom (SDOF). Two cases are considered: one is with a specimen of pure mass as shown Figure 1, and the other with a SDOF dynamic specimen as shown Figure 2.

3.1. Pure Inertia Specimen

When the experimental substructure is just an inertia mass, its reaction force at the *i*th step is easily obtained as

$$R_{\mathrm{E},i} = M_{\mathrm{E}}\tilde{a}_{\mathrm{C},i} \tag{3.1}$$

where $\tilde{a}_{\mathrm{C},i}$ is determined by Equation (2.6). Substituting Equation (3.1) into (2.4) yields

$$d_{i+1} = \left(\frac{M_{\mathrm{N}}}{\Delta t^2} + \frac{C_{\mathrm{N}}}{2\Delta t}\right)^{-1}\left[F_i - \left(K_{\mathrm{N}} - \frac{2M_{\mathrm{N}} - M_{\mathrm{E}}}{\Delta t^2}\right)d_i - \left(\frac{M_{\mathrm{N}} - 2M_{\mathrm{E}}}{\Delta t^2} - \frac{C_{\mathrm{N}}}{2\Delta t}\right)d_{i-1} - \frac{M_{\mathrm{E}}}{\Delta t^2}d_{i-2}\right] \tag{3.2}$$

Based on the above equation, the displacement responses of free vibration between two adjacent time steps can be related in a recursive form as

$$\mathbf{Y}_{i+1} = \mathbf{A}\mathbf{Y}_i \tag{3.3}$$

where $\mathbf{Y}_{i+1} = \begin{bmatrix} d_{i+1} & d_i & d_{i-1} \end{bmatrix}^{\mathrm{T}}$, $\mathbf{A} = \begin{bmatrix} -\frac{(1+\gamma_{\mathrm{m}})\Omega^2 - 2 + \gamma_{\mathrm{m}}}{1+\xi_{\mathrm{N}}\Omega} & -\frac{1-\xi_{\mathrm{N}}\Omega - 2\gamma_{\mathrm{m}}}{1+\xi_{\mathrm{N}}\Omega} & -\frac{\gamma_{\mathrm{m}}}{1+\xi_{\mathrm{N}}\Omega} \\ 1 & 0 & 0 \\ 0 & 1 & 0 \end{bmatrix}$, $\Omega = \Delta t\omega = \Delta t\sqrt{K_{\mathrm{N}}/(M_{\mathrm{N}} + M_{\mathrm{E}})}$,

$\xi_{\mathrm{N}}=C_{\mathrm{N}}/(2M_{\mathrm{N}}\omega)$, $\gamma_{\mathrm{m}}=M_{\mathrm{E}}/M_{\mathrm{N}}$. The matrix **A** is usually called amplification matrix and its eigenvalues determine the numerical behavior of an integration algorithm. In particular, the amplification matrix defines the stability condition of an integration algorithm through

$$\rho(\mathbf{A}) \le 1 \tag{3.4}$$

Where $\rho(\mathbf{A})$ is the spectral radius of **A**, which is defined as $\rho(\mathbf{A})=\max(\lambda_{\mathrm{i}})$, and λ_{i} are the eigenvalues of **A**. The characteristic equation of **A** can be obtained as

$$(1+\xi_{\mathrm{N}}\Omega)\lambda^3 + \left[(1+\gamma_{\mathrm{m}})\Omega^2 - 2 + \gamma_{\mathrm{m}}\right]\lambda^2 + (1-\xi_{\mathrm{N}}\Omega - 2\gamma_{\mathrm{m}})\lambda + \gamma_{\mathrm{m}} = 0 \tag{3.5}$$

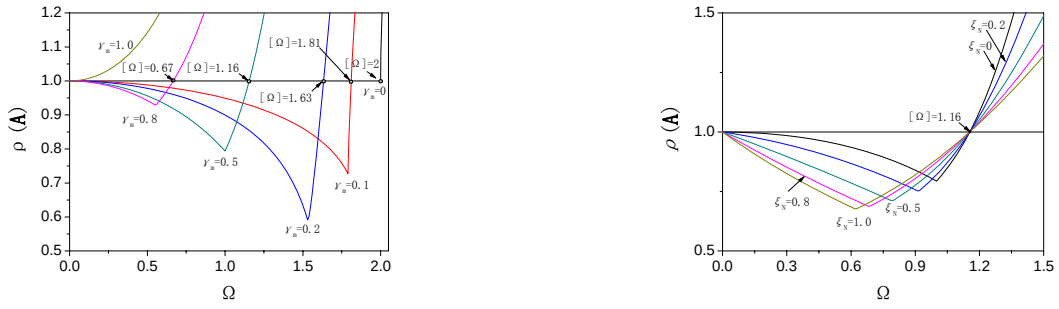

a) ξ_N=0 b) γ_m=0.5

Figure 3 Spectral radius of CDM for RST with pure inertia specimen

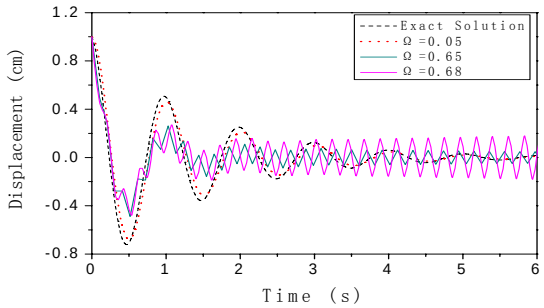

Figure 4 Free vibration responses with pure inertia specimen

We define a stability limit as the maximum of the Ω_s values such that $\rho(\mathbf{A})\leq 1$ for any $\Omega\in(0, \Omega_s)$. Letting $[\Omega]$ denote the stability limit, one may obtain the stability limit of the modified CDM for pure mass specimen as (Yang, 2007)

$$[\Omega] = 2\sqrt{\frac{1-\gamma_m}{1+\gamma_m}} \tag{3.6}$$

The above equation indicates that (i) the stability limit only exists when $\gamma_m<1$ (the non-existence of stability limit is called unconditionally unstable in this paper); (ii) the stability limit decreases with increasing γ_m; (iii) the stability limit has no relationship with damping from numerical substructure. The spectral radius $\rho(\mathbf{A})$ against Ω is plotted in Figure 3a with ξ_N=0 and different γ_m values. The stability limit values obtained from Figure 3a is identical to those calculated using Equation (3.6). Figure 3b shows the diagrams of spectral radius $\rho(\mathbf{A})$ against Ω with γ_m=0.5 and different ξ_N values. The independence of stability limit upon ξ_N is easily seen and is consistent with the observation from Equation (3.6).

The simulated displacement responses of free vibration with various Ω values are shown in Figure 4 where M_N=300kg, γ_m=0.8, ω=2π, ξ_N=0.2 and initial condition is d_0=1cm and v_0=0. The corresponding stability limit is 0.67 obtained with Equation (3.6). When Ω>0.67, the unstable response is observed in Figure 4. It is also seen that the simulated result approaches exact one with reducing Ω similar to standard CDM.

3.2. Dynamic specimen

For the RST of a structure as shown Figure 2 subject to seismic excitation, the reaction force $R_E(t)$ of the experimental substructure is only related to the acceleration $\tilde{a}_C$ (not $\tilde{d}_C$ or $\tilde{v}_C$) at the coupling degree-of-freedom through following equations.

$$R_{\mathrm{E},i}(t) = -\left(C_{\mathrm{E}} v_{\mathrm{E},i}(t) + K_{\mathrm{E}} d_{\mathrm{E},i}(t)\right) \tag{3.7}$$

$$M_{\mathrm{E}} a_{\mathrm{E},i}(t) + C_{\mathrm{E}} v_{\mathrm{E},i}(t) + K_{\mathrm{E}} d_{\mathrm{E},i}(t) = -M_{\mathrm{E}}(\tilde{a}_{\mathrm{C},i} + a_{\mathrm{g},i}) \tag{3.8}$$

in which a_{E}, v_{E} and d_{E} are the acceleration, velocity and displacement of experimental substructure relative to the numerical substructure, respectively; a_{g} is the ground acceleration; $t \in [t_{i-1}, t_i]$. Free vibration response of the experimental substructure is obtained using Duhamel's integral on Equation (3.8). Accordingly, the analytical solution of reaction force is derived. Its substitution together with Equation (2.6) into Equation (2.4) gives

$$d_{\mathrm{N},i+1} = c_1 d_{\mathrm{N},i} + c_2 d_{\mathrm{N},i-1} + c_3 d_{\mathrm{N},i-2} + c_4 d_{\mathrm{E},i} + c_5 v_{\mathrm{E},i} \Delta t \tag{3.9}$$

in which c_j's are constants related to structural parameters and time integration interval; their expressions can be found in Yang (2007). Letting

$$\mathbf{Y}_{i+1} = \left[d_{\mathrm{N},i+1} \quad d_{\mathrm{N},i} \quad d_{\mathrm{N},i-1} \quad d_{\mathrm{E},i} \quad v_{\mathrm{E},i}\Delta t \right]^{\mathrm{T}} \tag{3.10}$$

one may easily get the corresponding amplification matrix **A**.

It is difficult to obtain the analytical expression of spectral radius of the matrix **A** due to mathematical complexity. Therefore, the numerical analyses were carried out to investigate the spectral characteristics. Figure 5a shows the results of undamped cases with frequency ratio γ_ω equal to 1, where $\gamma_\omega = \omega_{\mathrm{E}}/\omega_{\mathrm{N}}$, $\omega_{\mathrm{E}} = \sqrt{K_{\mathrm{E}}/M_{\mathrm{E}}}$, $\omega_{\mathrm{N}} = \sqrt{K_{\mathrm{N}}/M_{\mathrm{N}}}$; the horizontal coordinate is defined as $\Omega = \omega_{\mathrm{N}}\Delta t$. It is seen that the spectral radius is always greater than unity, indicating unstable response, however small the mass ratio and Ω are. This means that the CMD is unconditional unstable for a dynamic specimen if there is no damping associated in the test structure. This contrasts the conditional stability of the case with pure mass specimen and the mass ratio lower than 1. Nonetheless the instability in the case of dynamic specimen is not that serious for small mass ratio and Ω since the spectral radius is very close to unity as shown in Figure 5a, if only the testing duration is not too long. It is also seen in Figure 5a that the instability is improved with reduced γ_{m}, as the spectral radius becomes closer to 1. The elimination of unconditional instability problem can be achieved by adding a damping to the structure. This is illustrated in Figure 5b where damping ratios of experimental and numerical substructures are both 5%, and γ_ω=1. The damping ratio here are defined as $\xi_{\mathrm{E}} = C_{\mathrm{E}}/(2M_{\mathrm{E}}\omega_{\mathrm{E}})$, and $\xi_{\mathrm{N}} = C_{\mathrm{N}}/(2M_{\mathrm{N}}\omega_{\mathrm{N}})$. Figure 6 shows the simulated and exact displacement responses of the free vibrations with $\xi_{\mathrm{E}} = \xi_{\mathrm{N}} = 0.05$, $\gamma_{\mathrm{m}} = \gamma_\omega = 1$. The initial conditions are: d_{N0}=1cm, d_{E0}=-1cm, $v_{\mathrm{N0}} = v_{\mathrm{E0}} = 0$. Different Ω's are considered in the simulation. The stability limit of this case is 0.44 from Figure 5b. It is observed from Figure 6 that the response is unstable when Ω= 0.45, which verifies the result of spectral analysis. Although the stable responses of RST are attained for smaller Ω's, the good agreement with the exact solution is seen only for an Ω as small as 0.05.

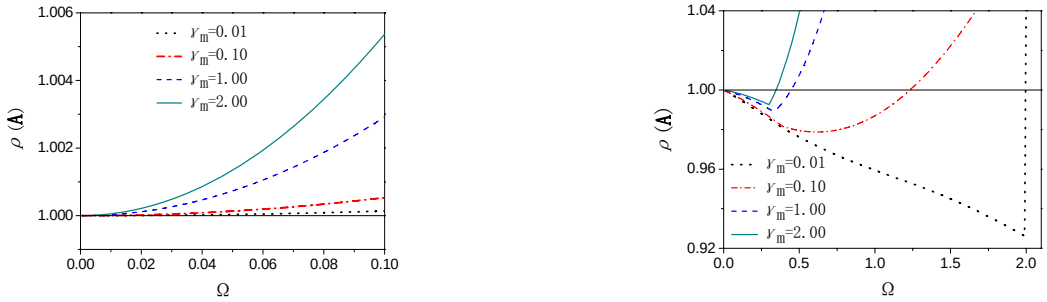

a) $\xi_{\mathrm{N}} = \xi_{\mathrm{E}} = 0$, $\gamma_\omega = 1$ b) $\xi_{\mathrm{N}} = \xi_{\mathrm{E}} = 0.05$, $\gamma_\omega = 1$

Figure 5 Spectral radius of CDM for RST with dynamic specimen

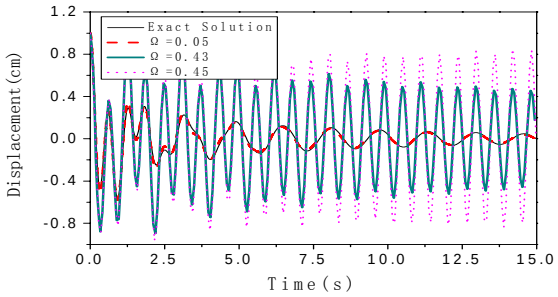

Figure 6 Free vibration responses with dynamic specimen

4. NUMERICAL SIMULATION OF RST WITH SHAKING TABLE

In Sections 2 and 3, the dynamics of physical loading system is not considered in order to emphasize the numerical behaviors of the algorithm itself. A shaking table is used in this section as a transfer system of the RST with dynamic specimen, and the stability performance will be investigated through some numerical simulations, in which the linear model of the Rice university shaking table developed by Conte et al. (2000) is adopted herein. All the parameters of the shaking table are the same as in Conte et al. (2000) except the control gains specified in this paper. The excitation is the El Centro (NS, 1940) earthquake record.

4.1. Pure Inertia Specimen

The parameters of the numerical substructure and experiment substructures for the numerical simulations are: M_N=300kg, ω=2π, K_N=(M_E+M_N)ω^2, C_N=0, M_E=M_N, and K_E=C_E=0. The period of the whole structure is 1 second. The PID control gains are K_P=0.394×5V/cm, K_I=0, K_D=0.085V·cm, and the feed-forward and differential pressure control gains are: K_{ff}=0.012V·cm and K_{dp}=-2.15×10^{-7}, respectively. The numerical simulation results with different mass ratios and the exact solution of the displacement responses are shown in Figure 7. The exact solution is calculated by using Lsim command in Matlab with the integration time interval of 0.01s. It is seen that the response becomes unstable when γ_m =1.003. This is consistent with the results of theoretic analysis in Section 3. It is also seen that the response approaches the exact solution with smaller γ_m.

4.2. Dynamic Specimen

The parameters of the numerical substructure, as shown in Figure 2, are M_N=500kg, ω_N=2π, K_N=$M_N\omega_N^2$, and ξ_N=0.05. The parameters of the experiment substructure are identical to the numerical substructure, i.e. γ_m=γ_k=γ_c=1. The PID control gains of the shake table controller are K_P=0.394×5V/cm, K_I=0, K_D=0.0725 V·cm, and the feed-forward and differential pressure control gains are K_{ff}=0.0125 V·cm and K_{dp}=-2×10^{-7}, respectively. According the analysis of Section 3, the stability limit is equal to 0.44 in this case. The displacement responses of the numerical substructure with different Ω values are shown in Figure 8. The unstable response is clearly seen when Ω=0.471>[Ω]=0.44. The better result is obtained as expected with smaller Ω.

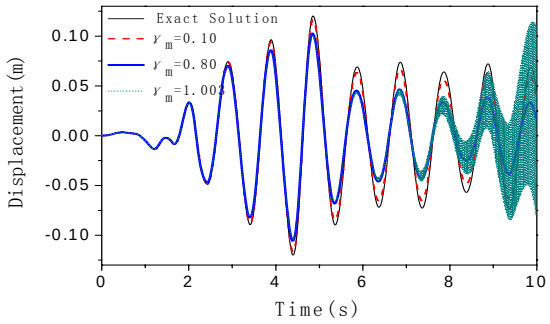

Figure 7 Numerical Simulation result of RST using shaking table (pure inertia specimen)

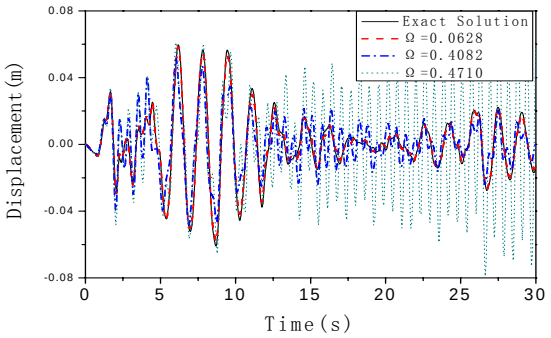

Figure 8 Numerical Simulation result of RST using shaking table (dynamic specimen)

5. VALIDATION TEST

A validation test was carried out at the Mechanical and Structural Testing Center of the Harbin Institute of Technology. The computation schematic of the whole test structure is shown in Figure 1. The experimental substructure was a pure mass made of cast iron with M_E=116kg. A photograph of the experimental substructure installed on the MTS servo-hydraulic actuator is shown in Figure 9. The parameters of the numerical substructure are $\omega_N=2\pi s^{-1}$, $K_N = M_N\omega_N{}^2$ and $C_N=0$. The integration time interval was 0.01. Figures 10-12 show the displacement commands and responses of free vibration with different mass ratios. The initial conditions are $d_0=0$, $v_0=3.14$cm/s. The displacement responses tracked the commands very well in all these cases as shown in Figure 10-12. The stable result was obtained with $\gamma_m=0.1$ and the decaying response is observed in Figure 10, probably due to the friction force between the guiding columns and the iron mass. With this friction force, the response remained stable with γ_m =1.01>1 as seen in Figure 11. Further increasing γ_m by reducing the mass of numerical substructure resulted in an unstable tendency of response as seen in Figure 12. The test was terminated before it went violently. Although the test results were not exactly the same as predicted by the analytical work in the previous sections, the influence of the specimen mass on the stability of RSTing with the CDM has been confirmed.

Figure 9 Photograph of test setup for RST

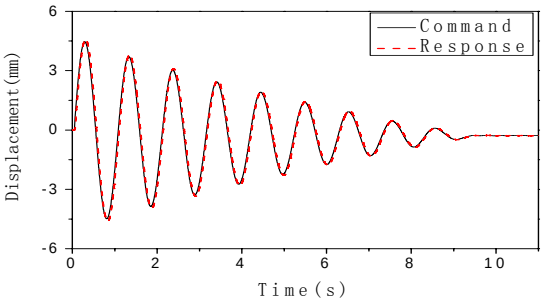

Figure 10 Test result with γ_m=0.1

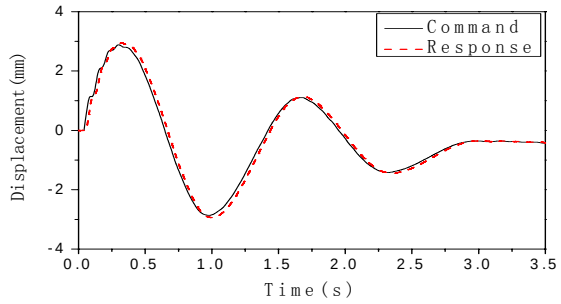

Figure 11 Test result with γ_m=1.01

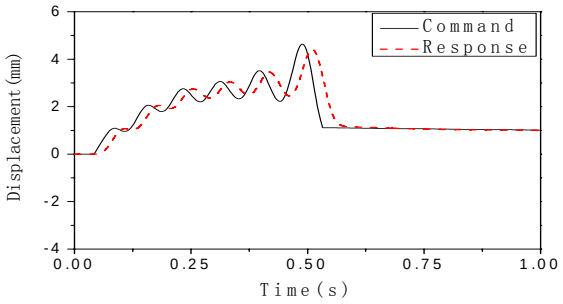

Figure 12 Test result with γ_m=1.3

6. CONCLUSION

The CDM is modified with an explicit acceleration formulation to obtain correct reaction force of dynamic specimen in a RST. The analytical work, numerical simulation of the RST with a shaking table and actual test have all shown that the stability of the algorithm decreases with increasing mass ratio of experimental over numerical substructures.

ACKNOWLEDGEMENTS

This work was supported by Grant 90715036 and 50578047 from the National Science Foundation of China, and China Ministry of Education through Program for New Century Excellent Talents in University. Mr. Y. Ma of the Mechanical and Structural Testing Center, Harbin Institute of Technology, is gratefully acknowledged for his assistance with the operation of the MTS testing system.

REFERENCES

Bursi, O.S., Gonzalez-Buelga, A., Vulcan, L., Neild, S.A. and Wagg, D.J. (2007). Novel coupling rosenbrock-based algorithm for real-time dynamic substructure testing. *Earthquake Engineering and Structural Dynamics*. **37,** 339-360.

Conte, J.P. and Trombetti, T.L. (2000). Linear dynamic modeling of a uni-axial servo-hydraulic shaking table system. *Earthquake Engineering and Structural Dynamics*. **29(9)**, 1375～1404

Horiuchi T and Konno T. (2001). A new method for compensating actuator delay in real-time hybrid experiments. *Phil. Trans. R. Soc. Lond. A* **359,** 1893-1909

Nguyen, V.T. and Dorka, U. E. (2006). Application of digital technique in a control system for real-time sub-structure testing. 4th World Conference on Structural Control and Monitoring, San Diego, USA.

Williams, M.S. and Blakeborough, A. (2001). Laboratory testing of structures under dynamic loads: an introductory review. *Phil. Trans. R. Soc. Lond. A* **359,** 1651-1669.

Wu, B., Bao, H., Ou, J. and Tian, S. (2005). Stability and accuracy analysis of central difference method for real-time substructure testing. *Earthquake Engineering and Structural Dynamics*. **34,** 705-718.

Wu, B., Wang, Q., Shing, P.B. and Ou. J. (2007). Equivalent force control method for generalized real-time substructure testing with implicit integration. *Earthquake Engineering and Structural Dynamics*. **36,** 1127-1149

Yang, X. (2007). Numerical simulation of real-time substructure testing with shaking table, Dissertation for the Master Degree Engineering, Harbin Institute of Technology.